Perspective: AIChE 2008 Alan P. Colburn Award Winner

The Chemical Engineering of Low-Dimensional Materials

Geraldine L. C. Paulus, Steven Shimizu, Joel T. Abrahamson, Jingqing Zhang, Andrew J. Hilmer, and Michael S. Strano*

Dept. of Chemical Engineering, Massachusetts Institute of Technology, Cambridge, MA 02139

DOI 10.1002/aic.12628
Published online April 11, 2011 in Wiley Online Library (wileyonlinelibrary.com).

Keywords: low-dimensional materials, single-walled carbon nanotubes, graphene, thermopower waves, excitons, single-molecule detection, ion transport, electron transfer chemistry

Low-Dimensional Materials

Low-dimensional materials (LDMs) are a new class of materials, which have one or more physical dimension(s) constrained to the nanometer scale. This constraint implies that the electrons within them are confined to less than three dimensions, a property that imparts such materials with new and unusual properties, as well as new opportunities for novel engineering applications. The properties of low-dimensional materials are substantially different from those of their bulk counterparts, and their understanding requires the application of fundamental chemical engineering concepts. In studying such materials, the central focus has been on understanding their physical and chemical properties, and their potential technological applications. Examples of LDMs include two-dimensional (2-D) nanosheets, one-dimensional nanowires, nanotubes and nanorods (1-D), and zero-dimensional quantum dots (0-D), all of which showcase a whole new range of properties when compared to their three-dimensional (3-D) bulk equivalents, with the change in properties arising from quantum confinement and/or surface and interfacial effects.[1]

Quantum confinement effects appear when the confining dimension(s) is (are) on the order of the wavelength of the electron wave function. This implies that when electrons or holes (the absence of electrons) are moving, their mean free path is larger than the dimension of the quantum structure, which typically happens at the nanoscale. In general, solids have a defined spectrum of allowable electronic states, called the electronic density of states (DOS). The nanoscale confinement in LDMs brings about a transition from a continuous to a discontinuous DOS which results in a whole new set of physical, optical and chemical properties. For example, as a result of quantum confinement the electronic band gap of 0-D and 1-D semiconductors becomes size-dependent, leading to their use in many interesting photoelectronic applications, such as solar cells, light emitting diodes (LED) and diode lasers.[2–5] Electrical conductivity is typically expected to be lower for LDMs than for their bulk equivalents due to scattering from, e.g., wire boundaries, edge effects, and quantization of conductivity. Thinking about a nanowire: the thinner the wire is, the smaller the number of channels available for the transport of electrons.[6]

As dimensions of electronics keep getting smaller it is likely to encounter ballistic transport of electrons, meaning there is negligible resistivity in the medium due to scattering. It can be observed when the mean free path of the electron is much bigger than the dimensions of the medium it travels through. This phenomenon occurs at the nanoscale and is, thus, more likely to be observed in LDMs than in their bulk equivalents. InAs nanowires with a diameter of 50 nm have shown ballistic transport over a length scale of about 200 nm at room-temperature.[7] However, it is generally hard to observe ballistic conduction in nanowires at room-temperature due to edge effects: the dangling bonds present defects and act as scattering sites for the electrons.

Thermal energy is another area where LDMs exhibit unique properties. The energy is stored and transmitted in nanostructures using electrons and particularly phonons—quantized units of solid lattice vibration. Like electrons, phonons have allowable energy levels in the solid and a density of phonon states. Quantum confinement generally lowers the value of the thermal conductivity, but can increase the specific heat of LDMs compared to their bulk counterparts, due to increased boundary scattering and quantization of the phonon DOS. For example, compared to bulk Si, Si nanowires have a reduced thermal conductivity χ, a development important for thermoelectric applications.[8]

*This article resulted from an invitation to Professor Michael Strano to contribute a Perspective, based on his cumulative body of research that was recognized by the 2008 Allan P. Colburn Award for Excellence in Publications by a Young Member of the Institute

Correspondence concerning this article should be addressed to M. S. Strano at strano@mit.edu

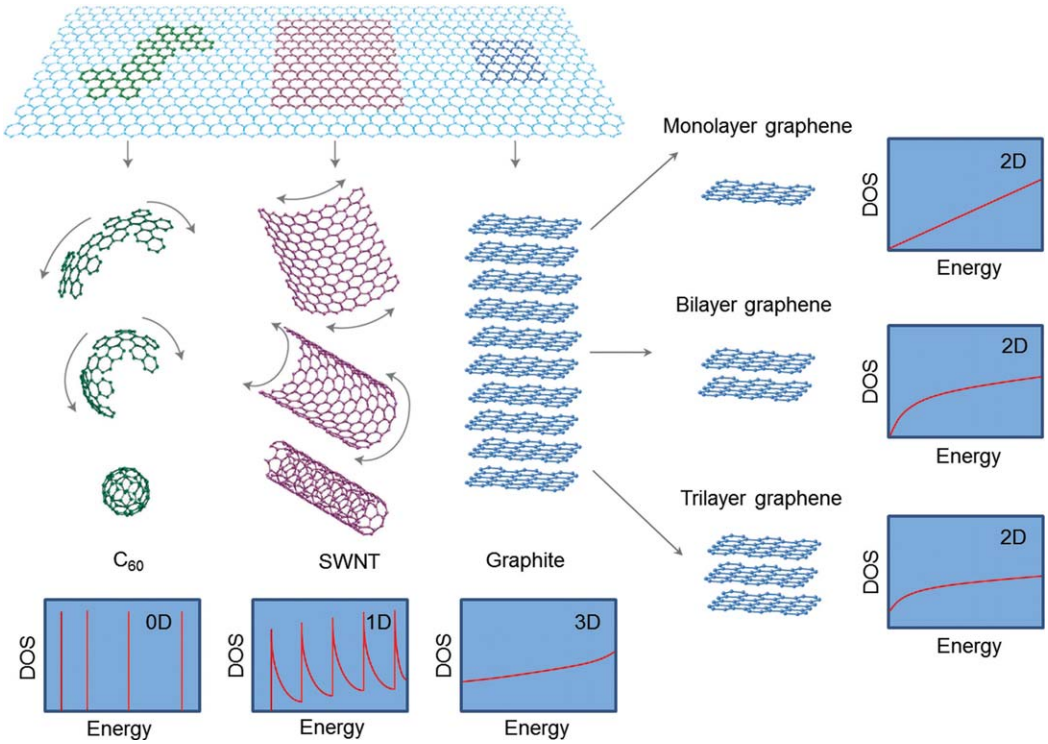

Figure 1. 2-D graphene (top panel) can be thought of as the building block of carbon materials of all other dimensionalities: 0-D buckyballs, 1-D carbon nanotubes, and 3-D graphite.

Reprinted in part with permission.[15] A qualitative density of states (DOS) of each material is included.

Nanowires are also great candidates for temperature sensors, as their conductance increases with increasing temperatures.[9]

Other shape, surface and interfacial effects characteristic of LDMs are very beneficial. A large surface-to-volume ratio is a big advantage that can be exploited for example in excitonic solar cells, where it is important to have a large interfacial contact area between the p-type and the n-type material. Other examples are size-, shape- and/or facet-controlled catalytic nanoparticles: their high surface-to-volume ratios, inherent energy of exposed atoms and surface-specific binding can lead to a high reactivity and selectivity.[10]

Most of the work by the authors of this Perspective over the past decade has focused on carbon as a unique precursor for low-dimensional materials. Graphene, for example, is a one-atom thick planar monolayer of sp^2-bonded carbon atoms organized in a hexagonal lattice (Figure 1). This material has been studied theoretically for more than 60 years,[11–12] but was never believed to exist in reality since all 2-D crystal structures were considered to be thermodynamically unstable.[13–14] Interest in graphene has exploded since the discovery of free-standing graphene and the demonstration that quasi-particles in graphene are massless Dirac fermions.[15] Andre Geim and Konstantin Novoselov were awarded the 2010 Nobel Prize in Physics for this work. Because graphene is a semimetal, it can be reduced to nanoscale dimensions without becoming an insulator, as is the case for many doped semiconductors.

Graphene can be thought of as the building block for carbon materials of all other dimensionalities (Figure 1). Three-dimensional graphite for example is essentially composed of stacked sheets of 2-D graphene. It was shown that the electronic structure of stacked graphene already approaches that of graphite at 10 layers.[16] This trend can also be observed by monitoring the DOS of graphene, bilayer graphene, trilayer graphene and graphite, schematically drawn in Figure 1.

Figure 1 also illustrates that graphene can be wrapped to form a 0-D bucky ball with a completely discrete DOS or rolled up to form a 1-D single-walled carbon nanotube (SWCNT) with discontinuous spikes in its DOS, known as Van Hove singularities (Figure 1). The angle along which the graphene sheet is rolled up and the tube diameter determine the exact form of the DOS of the resulting SWCNT, whether it is metallic, semimetallic or semiconducting, and the size of its band gap. The occurrence of the Van Hove singularities is the reason for many of the remarkable optical properties of SWCNT.

It is important to note that SWCNTs differ from nanowires in the sense that they are flexible, seamless hollow cylinders, whereas nanowires are solid cylinders, often with a larger diameter with many dangling bonds on their surface. Unlike most LDMs, carbon nanotubes exhibit a larger value of the thermal conductivity χ in comparison to that of their already very conductive bulk equivalent graphite, especially at low temperatures, since the interlayer interactions in graphite quench the conductivity by nearly an order of magnitude.[17] The absence of dangling bonds on their surface also results in greatly enhanced electric ballistic transport in SWCNTs compared to nanowires: ballistic length scales of up to 0.5 μm have been measured in SWCNTs at room-temperature,[18] making them ideal candidates for nanoelectronic applications such as field-effect transistors.[19] Moreover, given the high

transparency and flexibility of SWCNT-films[20] and graphene, they can be used as thin transparent flexible conductive electrodes.[21–22]

LDMs offer unique and exciting opportunities to chemical engineering both in terms of new science and innovative technologies. In an effort to present these opportunities as broadly as possible, this Perspective is organized as follows: the section "Heat Transfer at the Nanometer Scale: from Phonons to Thermopower Waves" presents a new energy generation mechanism, which is called *thermopower waves*. These self-propagating chemical reaction waves generate a thermal pulse that drives electrons down a conductive nanowire, for example, leading to fundamentally new types of batteries and fuel cells. The section "Exciton Engineering: the Next Frontier of Chemical Reaction Engineering" introduces the concept of excitons from a chemical engineering perspective and shows how reaction engineering concepts are essential in describing their behavior. This approach is applied to two state-of-the-art photoelectronic SWCNT-based applications. The section "Shrinking Chemical Sensors to the Nanometer Scale: Understanding Stochastic Fluctuations" describes how SWCNTs can act as a new class of chemical sensors capable of detecting and quantifying the flux of single molecules by monitoring the fluorescent decay of excitons generated on the nanotube. The section "New Developments in Mass Transport through Nanotube Pores" presents molecular transport through the interior of small diameter SWCNTs and illustrates that such nanopores demonstrate surprising and exotic behavior, namely a coherent molecular transport not predicted before by theory. These systems may lead to new separation membranes, sensors and nanoscale reactors. Finally, the section "The Electron Transfer Chemistry of One- and Two-Dimensional Materials" focuses on the chemical reactivity of SWCNTs, graphene nanoribbons (GNRs) and graphene, which is fundamentally influenced by the unique electronic DOS described in Figure 1.

Heat Transfer at the Nanometer Scale: from Phonons to Thermopower Waves

As mentioned previously, the thermal conductivity of carbon nanotubes is extremely high; at 3000—10000 W/m/K near room-temperature, it can be more than 10 times higher than that of copper. This implies that, if coated with exothermic fuel, they can channel heat from the resulting self-propagating chemical reaction wave to regions of unreacted fuel, accelerating the wave dramatically. The rapidly moving thermal gradient of the reaction wave also pushes a wave of charge carriers (electrons or holes) in the nanotubes, named a *thermopower wave*,[23,24] as depicted in the schematic of Figure 2. The polarity of the voltage generated depends on the majority charge carrier and the direction of the wave. Initiating the reaction on one end of a thermopower wave generator will produce a single-polarity electrical pulse, but initiation between the ends results in two waves traveling in opposite directions. The opposite signs of the voltage will then cancel each other to some extent, decreasing the power output. Regardless, the best thermopower wave generators exceed both the specific power (i.e., power per mass) of present-day battery technologies and the predictions of See-

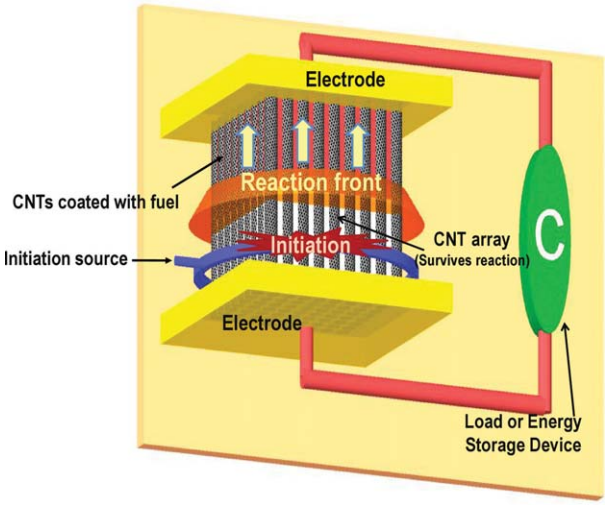

Figure 2. Schematic of a thermopower wave generator.

An array of thermal and electrical conduits, such as carbon nanotubes (CNT), is contacted on either end with electrodes and coated with exothermic fuel. A pulse of heat from a laser or a hot wire initiates a reaction wave, which propagates rapidly along the conduits in the direction of their highest thermal diffusivity. The conduits accelerate the reaction wave by supplying energy to unreacted fuel and survive the propagation of the wave. Adapted with permission.[23]

beck thermopower (assuming, an enormous temperature gradient of 2800 to 300 K, and a carbon nanotube Seebeck coefficient of 80 μV/K).

Abrahamson et al.[25,26] predicted with theoretical calculations that such highly conductive nanostructures can accelerate self-propagating reaction waves from an exothermic chemical reaction in close proximity. Remarkably, their large surface area-to-volume ratio can overcome the generally mediocre interfacial thermal conductivity between carbon nanotubes and fuels such that the nanotubes act as thermal conduits, rapidly conducting heat from the exothermic reaction to the unreacted fuel and accelerating the reaction wave along their lengths. Nair and Strano[27] continued to explore the theoretical limits of such systems by modeling fuel molecules attached to 1-D bead-spring arrays with harmonic or anharmonic potentials. In systems with very low-defect density, reaction waves can propagate faster than 8 km/s, provided that the largest portion of the enthalpy of reaction is coupled back into the bead-spring lattice (i.e., the nanoscale thermal conduit). However, these models also predict that if the activation energy for the decomposition of the fuel is less than 100 kJ/mol, the system becomes unstable and prone to unpredictable reaction independent of the initiating thermal pulse.

High-velocity reaction waves are not the only attractive outcome of the combination of an exothermic fuel and a nanoscale thermal conduit. If the nanostructure also possesses a large electrical conductivity (as metallic carbon nanotubes do with a value of 10000 S/cm), the thermal reaction wave can excite and push charge carriers along to create electrical current and voltage in a thermopower wave.[23–24] Experimental demonstration of these waves was achieved by coating multiwalled carbon nanotubes (MWCNTs) with cyclotrimethylene-trinitramine (TNA), and sodium azide (NaN_3). When initiated with a 300 mW laser, the resulting

reaction wave propagates faster than 2 m/s, which is more than 10,000 times faster than the reaction velocity in bulk TNA. The electrical pulses produced by the first thermopower wave generators, depicted in Figure 2, are as large as 7 kW/kg (or 250 mV), and the specific power was greatest in devices with the smallest mass — an unexpected inverse scaling. This exceptional power density in devices that can inherently be scaled down offers the promise that thermopower waves could power new microrobots and sensors, providing high-power pulses for long-distance communication and acceleration. They could also be useful as microthrusters, since the reaction produces an anisotropic pressure wave of high impulse per total system mass,[23] up to 300 N-s/kg.

The thermopower wave system can be modeled effectively as a 1-D system with heat diffusing according to Fourier's Law in a solid reactant with n^{th}-order reaction kinetics providing the energy source term, i.e.,

$$\rho C_p \frac{\partial T}{\partial t} = \chi \frac{\partial^2 T}{\partial x^2} - (\Delta H \cdot k_o Y) e^{-\frac{E_a}{RT}} \quad (1)$$

$$\frac{\partial Y}{\partial t} = -(k_o Y) e^{-\frac{E_a}{RT}} \quad (2)$$

where ρ is density, C_p is specific heat, T is temperature, t is time, χ is thermal conductivity, x is distance, ΔH is the reaction enthalpy k_0 is the Arrhenius prefactor, Y is the (mass) concentration of reactive material, E_a is the activation energy, and R is the universal gas constant. The solution provides the velocity of the resulting reaction wave and the form of the temperature and chemical conversion profiles by assuming that the temperature solution maintains the form of a generalized logistic function traveling at a constant velocity. This is confirmed by numerical simulation across a variety of conditions.[26]

For fuels with certain kinetic and thermal parameters, the numerical solution of the coupled reaction and thermal diffusion equations produces reaction waves with velocities that oscillate over time.[26] The model predicts the velocity frequencies to be in the range of 400–5000 Hz which is consistent with the voltage frequencies measured in the TNA-MWNT system described previously. This provides further evidence that the velocity of the reaction wave contributes to the thermopower voltage generated, beyond just the temperature difference. The velocity profile largely depends on the dimensionless parameter $\beta = \frac{C_p E_a}{-\Delta H R}$, i.e., the inverse adiabatic reaction temperature rise, that can be defined for each fuel. For $\beta \leq 6$, the amplitude of the velocity oscillations is negligible, and then as β increases linearly, so too does the amplitude. Importantly, the fundamental frequency depends on β with the form of an exponential decay, and the form of oscillations grows increasingly complex as β increases, transitioning around $\beta = 8$. For $\beta = 10.6$, which represents TNA, the oscillations have multiple significant frequency components. This diverse behavior provides rich opportunity for future study and offers potential applications for nanoscale signal processors or alternating current sources. Numerical simulation studies have shown that the oscillation parameters can be controlled by the choice of fuel for the thermopower wave.[26]

Unlike conventional thermoelectric generators, high-thermal conductivity leads to increased power output for thermopower waves.[23] In fact, the best thermopower wave generators produce several times more power than predicted by the Seebeck effect.[25] Simulation studies have shown that thermal conduits with larger thermal diffusivity accelerate the reaction wave more, and experiments have demonstrated that reaction wave velocity and specific power tend to be positively correlated.[23,25-26] Thus, high-Seebeck materials like silicon nanowires or bismuth telluride may not be the best conduits for thermopower waves, because their thermal diffusivities are low. The search for an optimum combination of Seebeck coefficient and thermal diffusivity to produce rapid, high-power thermopower waves remains a very active research interest of the authors.

Although present thermopower wave generators produce short electrical pulses—less than a second in duration—the maximum power density (> 7 kW/kg) can compete even with high-performance Li-ion batteries. Moreover, it surpasses many other energy technologies of similar size, including batteries, fuel cells, and energy harvesters.[23-24] Supercapacitors still produce the highest specific power, but their high self-discharge rate makes them impractical for long-term energy storage. On the other hand, thermopower waves generate their electricity from chemical energy in the bonds of fuel molecules, so they could remain stable for years. Fuel cells have a similar advantage in terms of energy storage, but tend to release energy at much lower rates than thermopower waves. However, since Raman spectroscopy confirms that the carbon nanotubes in thermopower wave generators survive the reaction, they could be refueled.

One key advance for the further development of thermopower waves will be expanding the fuels that can be used to include more common molecules like gasoline, ethanol, methane, or formic acid. This will make them more economical and simplify refueling. Another important challenge is increasing the efficiency of chemical-to-electrical energy conversion. Systems engineering and design will provide the tools to reduce thermal losses, particularly from radiation, which is the largest factor because of the high-reaction temperatures ($\sim$ 1000 K).

The authors continue to investigate what properties are responsible for the excess power beyond the Seebeck limit that has been measured. The answer may be found in the strong electron-phonon coupling in carbon nanotubes,[28] which could lead to the charge carrier entrainment effect. As one establishes the physical principles for thermopower wave propagation, the design rules to produce more efficient, higher power, versatile thermopower wave generators will be uncovered.

Exciton Engineering: the Next Frontier of Chemical Reaction Engineering

Excitons are electron-hole quasiparticles that are central to the operation of most photovoltaics and certainly many photocatalytic processes.[29] They form when an electromagnetic wave interacts with many types of matter. The separation of the exciton into electrons and holes is the source of usable electrical energy in a polymer heterojunction photovoltaic cell for example, or a dye-sensitized solar cell. The diffusion of excitons to an engineered interface that can subsequently split them into electrons and holes remains a central challenge in many polymer and nanocomposite photovoltaic cells.

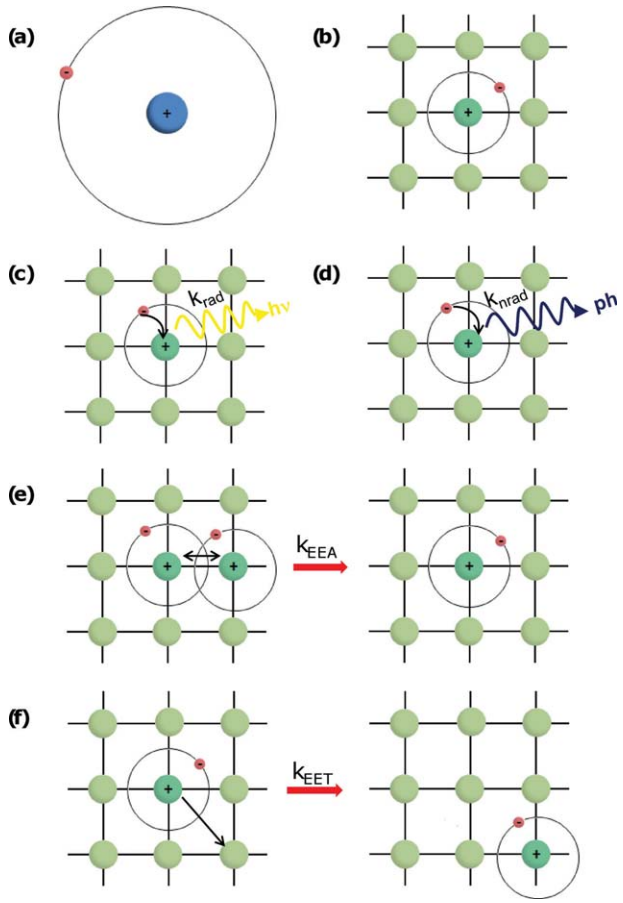

Figure 3. "Reactions" involving excitons.

(a) Conceptually, an exciton is similar to a hydrogen atom: one electron orbiting one proton, bound together by Coulomb interactions. (b) For comparison, a Frenkel exciton in a lattice: one electron was promoted from the valence band to the conduction band leaving behind a localized positively-charged hole. Coulomb interactions are relatively strong in low-dielectric materials. However, the binding energy is smaller and the particle size is larger than that of a hydrogen atom due to dielectric screening. (c) A first order decay reaction: radiative recombination of an exciton, giving rise to photoluminescence. (d) Another first order decomposition reaction: defect-mediated nonradiative decay giving rise to a phonon. (e) A second order reaction: exciton-exciton annihilation (EEA) where upon the collision of two excitons one is annihilated, whereas the other uses the energy from the collision to be promoted to a higher energy level. (f) Exciton energy transfer (EET), which can be thought of as a form of diffusion.

However, while one may find many chemical engineers making significant contributions to the materials for solar energy systems, quite curiously, one notices little conceptual usage of the exciton in the work of a chemical engineer. This is peculiar, because unlike electrons or holes moving throughout a photovoltaic device, excitons are largely neutral. Chemical engineers tend to relegate the former particles to the electrical engineers and physicists for description, since an explicit accounting of charge is central to their modeling. The exciton, however, can be described using the same population balances, mass transfer and chemical kinetics approaches that chemical engineers know well and practice extensively. A good conceptual model for the exciton is a hydrogen atom with a positively charged electron vacancy (i.e., a hole) as the nucleus and an orbiting electron (Figure 3a and 3b). In materials with a low-dielectric constant (e.g., π-conjugated polymers) the Coulomb interaction between the electron and the hole may be significantly strong, and this leads to relatively small excitons, on the order as the size of a unit cell, with a typical binding energy of 0.1–1 eV. This type is called a Frenkel exciton and is relevant in organic photovoltaics and nanomaterials.[30] Because the exciton is small enough, it can be treated as a delocalized particle: the exciton has a diffusivity as it "hops" from lattice site to lattice site, and can "react" at certain interfaces to yield electrons and holes as important products. Excitons also "react" in the bulk in many first- and second-order reaction pathways. They can radiatively recombine, producing a photon. Many optically active nanostructures and polymeric materials will fluoresce and this process can be considered to have first-order kinetics. Excitons can nonradiatively recombine to produce lattice vibrations or phonons in a similar but distinct first-order process. Auger recombination, also referred to as exciton-exciton annihilation (EEA) involves second-order and higher kinetics since it involves multiple excitons. These reaction pathways are schematically presented in Figure 3c–f.

There are two ways in which engineers can simulate the behavior of excitons as conserved particles: via deterministic and stochastic models. A deterministic reaction-diffusion model for a system where an electromagnetic source is incident onto a film of an excitonic material can be represented by the following partial differential equation (PDE)

$$\frac{\partial N(y,t)}{\partial t} = G(y,t) + \frac{\partial^2 (D \cdot N(y,t))}{\partial y^2} - \frac{N(y,t)}{\tau} \tag{3}$$

where N represents the population of excitons in the film, which is a function of time t, and depth y in the film. The one-dimensionality implied by Eq. 3 is typical for symmetric domains. The term $G(y,t)$ represents the bulk generation rate of excitons as in the case of a continuous light source (e.g., the sun for solar cell applications). This term can be absent and replaced by an initial condition if the film is excited at time $t = 0$ with a short laser pulse in a pump-probe experiment for example. The diffusion coefficient D is defined conventionally for excitons in the domain. Diffusion has been reported to be thermally activated with reported values of 40–60 meV (i.e., 0.92–1.38 kcal/mol) for the activation barrier in π-conjugated polymer films.[31–32] The third term on the righthand side of Eq. 3 lumps all excitonic decay channels, and is characterized by the exciton lifetime τ in the material, where $\tau = 1/k$ and k is the exciton decay rate constant. For π-conjugated polymers the exciton lifetime is typically on the order of 100 ps.[33] This lifetime is dominated by nonradiative decay (the radiative exciton lifetime is only on the order of $\sim$1ns).[33] The excitonic decay shows Arrhenius decay with activation energies reported from 15–120 meV (i.e., 0.35–2.77 kcal/mol).[31–32,34–36] Depending on the boundary conditions (e.g., quenching of excitons at interfaces with other materials), the solution to Eq. 3 will be of a different form.

One can define a diffusion length L_D for the excitons in the film

$$L_D = \sqrt{D\,\tau} \tag{4}$$

Table 1. Calculation of the Thiele Modulus for a 13 nm Thin Film of MDMO-PPV

Temperature T (K)	Lifetime τ (ns)	Diffusion Coefficient D (10^{-4}cm^2/s)	Exciton Diffusion Length L_D (nm)	Thiele modulus ϕ
4	0.60	1.4	2.9	4.5
50	0.62	1.5	3.05	4.3
100	0.59	1.6	3.1	4.2
150	0.65	1.6	3.24	4.0
200	0.63	2.0	3.55	3.7
250	0.69	2.3	4.0	3.3
293	0.63	3.2	4.5	2.9

The MDMO-PPV is spun from solution on top of a crosslinked fullerene layer, called poly(F2D) that serves as the exciton quenching wall. In order to measure the PL decay, samples were excited by a 100fs pulsed Kerr mode locked Ti-sapphire laser, frequency doubled at about 400 nm.[37]

This value represents the average distance an exciton can "travel" in the material within its lifetime τ, and is typically measured in different materials and at different temperatures by monitoring the decay of photoluminescence (PL) after excitation at $t = 0s$ using time-resolved spectroscopy.

Another typical chemical engineering parameter that is amenable to the system of reacting and diffusing excitons is the Thiele modulus, which can be compared across several materials and systems. This parameter arises from the nondimensionalization of Eq. 3 and considers the length scale of the domain L, in which the exciton is free to diffuse. This can be the thickness of the polymer film, a polymer domain in which the exciton resides, or the length of a nanotube along which the exciton migrates in 1-D. The Thiele modulus ϕ of excitons can be defined as the square root of the ratio of the reaction rate to the diffusion rate

$$\phi = \sqrt{\frac{kL^2}{D}} = \sqrt{\frac{L^2}{\tau D}} \tag{5}$$

As an example the authors of this Perspective calculated the Thiele modulus as a function of temperature for a system described in literature: Mikhnenko et al. extracted the exciton lifetime τ in a thin film (13 nm) of MDMO-PPV ((poly[2-methyl-5-(3′,7′-dimethyloctyloxy)-*p*-phenylenevinylene]) at different temperatures by performing PL decay experiments as described earlier.[37] By solving Eq. 3 they obtained a value of the diffusion coefficient. This diffusion coefficient is related to the exciton diffusion length via Eq. 4. Table 1 shows the main parameters as a function of temperature. In the last column the Thiele modulus is calculated based on Mikhnenko's data. It is clear that as the temperature increases the Thiele modulus becomes smaller and the system evolves from diffusion-controlled toward reaction-controlled, although the modulus remains of order 1.

In reality, reaction and diffusion of excitons happen on a molecular level and are stochastic in nature. Therefore, excitonic systems can often be represented by a kinetic Monte Carlo (KMC) simulation, where the probability of an event occurring is calculated within a certain time span. Stochastic models are usually adopted when there is a small number of excitons, N in the system and fluctuation is unavoidable. In the limit of large values of N, the average result of the stochastic simulation will converge to the deterministic result.

In these Monte Carlo simulations excitons are generated at the different lattice sites at rates determined by the incident light intensity and spectrum, as well as by the optical properties of the excitonic material itself. Once an exciton is generated, the simulation tracks its path. Each different event described earlier (radiative combination, nonradiative recombination or diffusion) can be characterized by a waiting time τ_w that depends on its actual rate constant k

$$\tau_w = -\frac{1}{k}\ln(X) \tag{6}$$

where X represents a random number in the interval [0,1]. For each exciton generated, the waiting time for all different events is calculated and the event with the smallest waiting time is selected to occur.

Although the migration of excitons in solids and nanoparticles is often described by Fickian diffusion in the deterministic approach, formally, an exciton "hops" to another point in space because the local oscillation of its electric field creates a new exciton at some other point in the matrix. This exchange, called exciton energy transfer (EET), is stochastic in nature, and, hence, is easily amenable to description by kinetic Monte Carlo simulation. The transfer is biased toward portions of the material that have lower energy states. Typically, a hopping rate k_{ij} constant is defined

$$k_{ij} = k_0 f(r_{ij}) \begin{cases} 1 & \text{if } E_i - E_j > 0 \\ \exp\left(\frac{-\Delta E_{ij}}{k_B T}\right) & \text{if } E_i - E_j \le 0 \end{cases} \tag{7}$$

where k_0 is the attempt-to-escape frequency, E_i and E_j are the energies of site i and site j, respectively, ΔE_{ij} is their difference, r_{ij} is the distance between the sites involved, k_B is the Boltzmann constant, and T is the temperature. Hopping is considered within the intrinsic density of states of the excitonic material. The functional form of $f(r_{ij})$ depends on the system under consideration. For bulk heterojunction (BHJ) solar cells for example, the hopping of excitons can be described by Förster resonance energy transfer (FRET).[38] In this case $f(r_{ij})$ takes the following form

$$f(r_{ij}) = \frac{1}{1 + \left(\frac{r_{ij}}{a}\right)^6} \approx \left(\frac{a}{r_{ij}}\right)^6 \tag{8}$$

where a is the Förster radius, defined as the value of the distance at which the hopping rate is equal to the decay rate (the energy transfer efficiency is 50%). This value depends on the overlap between the emission spectrum of the donor material and the absorption spectrum of the acceptor material. A donor chromophore, initially in its electronic excited state, can transfer energy to an acceptor chromophore (in proximity, typically less than 1 nm) through nonradiative dipole-dipole coupling. This expression is valid in bulk heterojunctions where the donor and the acceptor molecules are blended on a nanometer length scale.

However, in a planar heterojunction the donor and acceptor molecules are typically separated by much larger distances and the hopping trajectory of excitons between different sites of one material is better described by a random walk. In this case, $f(r_{ij})$ is best described with a Miller-Abrahams expression[39]

$$f(r_{ij}) = \exp\left(-2 \times \frac{r_{ij}}{\alpha}\right) \tag{9}$$

where α is the localization length of excitons in the excitonic material.

The macroscopically defined diffusion coefficient D can also be related to what happens at the molecular level

$$D = \frac{\langle r^2 \rangle}{2d\,t} \tag{10}$$

In this equation $\langle r^2 \rangle$ represents the mean-square displacement of the exciton during the time-interval t, two parameters which can easily be predicted by the kinetic Monte Carlo simulation. Note that d represents the dimensionality of the system ($d = 1,2$ or 3).

There are many reaction engineering applications of exciton transport and reaction, and these concepts have driven and guided key aspects of the work by the authors of this Perspective, as is demonstrated by the following recently published examples.

Polymer nanoheterojuction photovolatics

There is significant interest in combining carbon nanotubes with semiconducting polymers for photovoltaic applications, due to potential advantages from smaller exciton transport distances and enhanced charge separation. Since exciton diffusion to an interface capable of dissociating it into electrons and holes, such as a p-n junction, is often the bottleneck in photovoltaic performance, one idea is to use an anisotropic material such as a nanotube or nanowire that is capable of dissociating the exciton at its surface and transporting the resultant free electron to the cathode. In reaction engineering terms, this is analogous to circumventing diffusion controlled reaction by increasing the catalytic surface area. In the case of carbon nanotubes, however, bulk heterojunction (BHJ) devices have demonstrated extremely poor efficiencies for reasons that were not quite understood,[40–41] since their fullerenic counterparts, such as C_{60} and PCBM, and their derivatives, are very efficient electron acceptors and used routinely in BHJ devices.

Since little is understood about the nanotube/semiconducting polymer interface, Ham et al. constructed a planar nanoheterojunction photovoltaic device comprised of well-isolated mm-long SWCNTs underneath a poly(3-hexylthiophene) (P3HT) layer.[42] In this simple configuration, the resulting junctions displayed photovoltaic efficiencies per nanotube ranging from 3–3.82%, which exceed those of polymer/nanotube BHJ by a factor of 50–100. The increase is attributed to the absence of aggregate formation in this planar device geometry. Aggregates of carbon nanotubes appear to enhance the recombination of excitons before they can dissociate at the polymer/nanotube interface. Most of the photocurrent observed is that which is generated at the polymer/nanotube interface from exciton dissociation. Typical open-circuit voltages are near 0.5 V with fill factors of 0.25–0.3, which are largely invariant with the number of nanotubes per device and P3HT thickness.

Interestingly, a maximum photocurrent and efficiency for a 60 nm thick P3HT-layer was observed, in contradiction to an expected value equal to the diffusion length of excitons in P3HT (8.5 nm).[43] A similar maximum has been observed in another state-of-the-art P3HT-based planar heterojunction, where the acceptor material is PCBM.[44] In an effort to investigate and predict this curious behavior with a model Paulus et al. combined an optical T-matrix model with a KMC simulation to investigate photocurrent generation.[45] These PHJs are typically multilayered stacked devices; the optical T-matrix model takes the thickness of each layer, and the real and imaginary parts of the refractive index of each material in the device as an input, thereby taking into account effects of optical interference possibly occurring at each interface in the device.[46] The result of the optical model (the generation rate of excitons as a function of position in the device) then serves as the input for a first reaction model, a specific type of KMC, where bimolecular interactions of the excitons are neglected; a valid assumption for illumination under standard AM 1.5 G conditions.[47] The model demonstrates how a bulk exciton sink can explain this shifted maximum in the P3HT/SWCNT case, whereas the maximum is mainly determined by PCBM interdiffusing in P3HT in the P3HT/PCBM case.

Based on the results of this model it will be possible to more intelligently design polymer hybrid solar cells (both planar and bulk), and optimize them towards higher efficiencies.

Exciton Antennas

Developing new photonic materials for optical concentration and photon collection is crucial for applications such as higher efficiency photovoltaic cells and infrared photoemitters/photodetectors. One-dimensional materials such as single-walled carbon nanotubes are promising candidates due to their aligned axial transition dipoles, large absorption cross sections and high-quantum efficiencies. Photonic applications of SWCNTs, however, have always been hampered by their tendency to aggregate in bundles of inhomogeneous composition and our previous inability to isolate optically distinct species. Recent advances have enabled this separation on preparative scales.[48–50] Han and Paulus et al. recently dielectrophoretically assembled SWCNTs of homogeneous composition into aligned filaments giving rise to strong photoluminescence (PL).[51]

By engineering these filaments in a unique way one can take advantage of the aforementioned described Förster resonance energy transfer (FRET), where excitons residing on SWCNTs with a larger band gap are prone to transfer their energy to excitons located on SWCNTs with a smaller band gap.[52] These filaments consist of an annular shell of larger band gap (6,5) SWCNTs ($E_g = 1.21$ eV) surrounding a core of a variety of smaller band gap SWCNTs ($E_g = 1,17$ eV for (7,5) SWCNTs to 0,98 eV for (8,7) SWCNTs). Despite broadband absorption in the ultraviolet-near-infrared wavelength regime experimental results indicated quasi-singular photoemission at the a wavelength that corresponds to the E_{11} band gap of the (8,7) SWCNT (the SWCNT with the smallest band gap in the filament). Since these lowest band gap SWCNTs are located in the center of the filament, light has essentially been concentrated, both energetically and spatially. As better separation of different SWCNT chiralities becomes possible, it will be possible to engineer fibers such that light is focused to a desired wavelength, which may vary depending on the application.

The experimental data also reveal an unusually sharp, reversible decay in photoemission that occurs as such filaments are cycled from ambient temperature to only 357 K.[51] Han and Paulus et al. set up a deterministic model taking into account exciton generation, FRET from larger band gap to

Table 2. Rate Constants in SWCNT Filaments Created by Han and Paulus et al.[51]

Order of process	Exciton Reaction Rate Constant
1st	$k_{rad} \approx 10^7\ s^{-1}$
1st	$k_{FRET} \approx 6.25\times10^9\ s^{-1}$
1st	$k_{nrad} \approx 10^{10}\times\exp(-0.17/k_BT)\ s^{-1}$
2nd	$k_{EEA} \approx 10^{10}\times\sqrt{T}\times\exp(-0.20/k_BT)\ s^{-1}$

In the expressions k_B is the Boltzman constant and T the temperature.

smaller band gap SWCNTs, radiative and nonradiative decay of excitons in the SWCNT filaments and fit it to their PL experimental data.[51] Table 2 shows the values the different rate constants. The radiative rate constant k_{rad} and the FRET rate constant k_{FRET} show little temperature dependence in the range considered. The defect-mediated nonradiative rate constant k_{nrad} follows classical Arrhenius-behavior and the exciton-exciton annihilation rate constant k_{EEA} is modeled with collision theory, resulting in modified Arrhenius expression with a temperature-dependent prefactor. This prefactor indicates that as the temperature increases, two excitons residing on the same SWCNT diffuse faster along the length of that SWCNT, increasing chances of a collision. This strongly temperature-dependent second-order EEA process is responsible for the PL quenching at elevated temperatures.

These results have conclusively demonstrated the potential of specifically designed collections of nanotubes to manipulate and concentrate excitons in unique ways.

Shrinking Chemical Sensors to the Nanometer Scale: Understanding Stochastic Fluctuations

SWCNTs are used ubiquitously as various kinds of chemical sensors, where fluorescence-based detection emerges as a particularly advantageous modality, mainly due to its high sensitivity,[53] high-quantum efficiency,[54] and indefinite photostability.[55] In addition, compared to conventional small molecule fluorophores, nondiffusive SWCNTs allow for the otherwise impossible detection of single molecules with precise spatial resolution at the nanometer scale. Figure 4 gives an example of such a detection scheme where the array of SWCNTs responds to the analytes of interest locally, with each sensor in the array showing fluorescence quenching or enhancement due to the adsorption or desorption of the molecule, respectively, thereby and of, reporting an individual measurement. This provides promises of probing and quantification of highly reactive and unstable molecules of interest from local generation sources, such as a single immobilized cell, with nanometer resolution.

Jin et al.[53] and Zhang et al.[56] have reported detection of reactive oxygen/nitrogen species (ROS/RNS) such as hydrogen peroxide (H_2O_2), and nitric oxide (NO), using an array of selective SWCNT sensors. An emerging concept in cell signaling is the natural role of reactive oxygen species, such as hydrogen peroxide (H_2O_2), which functions as a messenger in many signaling pathways. Despite the growing research effort, there are still difficulties in tracking the generation of H_2O_2 in living systems, especially in terms of resolving it in a spatiotemporal manner. Jin et al.[53] developed a sensing platform, which is composed of an array of sensors constructed with collagen-wrapped SWCNTs. This configuration is capable of real-time recording of the stochastic quenching events that occur when H_2O_2 molecules are released from individual human epidermal carcinoma cells upon exposure to the epidermal growth factor (EGF). When no cells are placed onto the collagen-SWCNT film, no fluorescence quenching is observed; SWCNT sensors near or under plated A431 cells show discrete quenching transitions measured by a number of counts per unit time, which is attributed to the H_2O_2 originating from cellular metabolic activity as well as from nonspecific receptor-ligand binding. Upon exposure to EGF, such arrays have the ability to distinguish between membrane generation of H_2O_2 and other contributions.

Another SWCNT-based sensing platform comprises of an array of a specific sequence of DNA-suspended SWCNTs, which is capable of reporting distinctly selective single-molecule adsorption and desorption of NO molecules.[56]

It is possible to extract useful chemical information from the stochastic counting of single molecules, in order to generate useful information for problems in biology and catalysis. A birth-and-death Markov model can be constructed to describe the experimental quenching traces of single-molecule counting, from which the maximum likelihood estimator of both adsorption and desorption rates can be derived. More

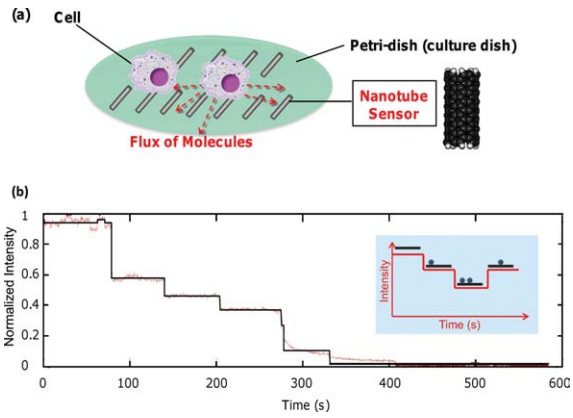

Figure 4. (a) Schematic of the cellular application of a SWCNT sensor array. An array of SWCNTs can be placed directly underneath the cells, with each sensor individually quantifying the concentration of the molecule locally with nanometer-scale spatial resolution. The fluorescence of each sensor responds to the adsorption of the molecule, showing either quenching or an enhanced response. (b) A typical time-trace of fluorescence response of a diffraction-limited spot (2×2 pixels) in a nIR microscope image after the SWCNT being exposed to NO (t = 0s) at the concentration of 3.9 μM and fitted traces (Chi-squared error-minimizing step-finding algorithm, black).

Each trace is normalized by the difference between the starting intensity and the dark-current intensity, and the latter is obtained through averaging intensity over a 20×20 pixel spot that does not contain any SWCNTs. Inset: Schematic of the fluorescence response of a single SWCNT; adsorption of a single quencher molecule of the analyte decreases the fluorescence by one step, whereas desorption of the single quencher molecule increases the fluorescence by one step. The stepwise intensity change can be recorded over time.

specifically, a single SWCNT is described by N contiguous segments, each of which is approximately the size of the exciton-diffusion length.[57–59] At any instant, the following reaction occurs

$$\mathrm{NO} + \theta \underset{k_d}{\overset{k_a}{\leftrightarrow}} \theta^* \tag{11}$$

where k_a and k_d are defined as the single-site adsorption and desorption rates of NO, respectively. θ and θ* refer to empty and NO-occupied sites on the SWCNT, respectively. Mass action of reaction (11) leads to

$$\begin{aligned} &\frac{d\theta}{dt} = -(k_a[\mathrm{NO}])\theta + k_d(\theta^*) \\ &\theta + \theta^* = N \end{aligned} \tag{12}$$

where N is the total number of sites on the SWCNT. The bulk concentration of NO is assumed to remain constant by $k_a[\mathrm{NO}] = k_a^{'}$ = constant. While both $k_a^{'}$ and k_d will affect the fluorescence response, $k_a^{'}$ is more important because it provides a direct measure of NO concentration, which determines both the degree of quenching of the fluorescence over the observation time, and the rate.

The ability to detect nitric oxide quantitatively at the single-molecule level may find applications in new cellular assays, such as studies of NO related carcinogenesis and inflammation diagnostics.[56]

New Developments in Mass Transport through Nanotube Pores

An important goal of nanotechnology is the ability to actively manipulate and transport single molecules, which would pave the way for nanoscale reactors and conduits as well as for novel separation systems. Among their many interesting properties, carbon nanotubes are atomically smooth and straight-line pores that can be used to control mass transport on an extremely small scale. Despite having a hydrophobic interior, it has been demonstrated both theoretically[60–61] and experimentally[62–63] that water will spontaneously fill carbon nanotubes due to confinement effects, forming a hydrogen-bonded, 1-D water chain through the nanopore, which makes it possible to use them in nanofluidic systems.

Recently, there have been several experimental studies which analyzed the transport properties of aligned nanotube membranes, which have shown fast mass transport of water through nanotubes,[64] ion selectivity,[65] and the ability to change selectivity based on end-group functionalization.[66] There have also been studies of transport through single solid-state nanopores, which are very short in length, have charged interiors, and are generally conical.[67–69] However, the experimental analysis of transport of ions through individual carbon nanotubes has not been studied in depth.

Lee et al.[70] and Choi et al.[71] have pioneered a platform to probe single ion transport through single-walled carbon nanotubes through Coulter detection of single cations (Li^+, Na^+, K^+). The fabrication process, depicted in Figure 5, consists of growing horizontally-aligned, ultra-long SWCNTs ($\sim$1 cm long) on a silicon substrate with an average diameter of 1.5 nm using chemical vapor deposition (CVD). A thick epoxy structure containing reservoirs and a very thick barrier (500–1000 μm in width) is bonded to the surface using UV glue. A very thick barrier is necessary to reduce leakage current to extremely low levels. This epoxy structure also serves as a mask in order to etch away the exposed nanotubes on either end of the barrier. The final device consists of reservoirs that are connected only by nanotubes of extremely high-aspect ratios (250,000–500,000).

A voltage clamp setup was used to probe the transport of charged species in solution, in which the apparatus maintains a constant voltage across two reservoirs, and simultaneously measures the resulting current required to sustain that voltage. This analysis technique has typically been used in biology to study ion transport through biological pores, which tend to be either in a conducting or non-conducting state. Biological pores can change between these two states through a change in conformation initiated by some analyte molecule, for example, which results in traces with discrete current states.

When voltage clamp measurements are performed on SWCNTs spanning two reservoirs, one also observes discrete current states. Unlike biological pores, these current states cannot be attributed to changes in nanotube conformation, as it is a passive and immobilized pore. Instead, it has been proposed that the discrete current states observed are due to cations blocking an otherwise stable proton current.[70] Thus, the high-conducting state is due to fast proton transport through an unobstructed nanotube, and the low-conducting state is due to a cation species blocking a significant portion of proton transport of ions. This stochastic pore blocking phenomenon allows indirect observation of single-ion transport events across a SWCNT. Although several SWCNTs span the barrier, as seen in a scanning electron microscope, only two states are observed, corresponding to one open SWCNT; the other SWCNTs may be broken or completely blocked by nanoscale debris.

It should be noted that this pore blocking phenomenon has neither been predicted nor ruled out theoretically, as molecular dynamics simulations are on the order of nanoseconds, as opposed to tenths of a second required in the aforementioned described system. In order to observe partitioning of ions into the SWCNT at the former time scale, the applied electric fields would have to be many orders of magnitude higher than possible in our experimental setup.

The evidence for this stochastic pore blocking phenomenon is summarized in Table 3. The hypothesis that protons are the majority carriers is supported by the fact that the pore blocking current (the current difference between states) decreases with increasing pH (lower proton concentration). Furthermore, when D_2O was used, the pore blocking current decreased due to the lower mobility of the higher-mass deuterium ions. Theoretically, proton translocation occurs by the Grotthuss mechanism, where protons hop from one water molecule to the next, rather than by molecular diffusion,[72] allowing the mobility to be an order of magnitude higher in this confined nanoscale regime than in the bulk.[73]

Water or solutions of HCl themselves exhibit only a single current state, so that the cations in solution must contribute somehow to the discrete current states. Furthermore, conductivity measurements show that the addition of salt actually *lowers* the conductivity, meaning it is inhibiting the main charge carriers. The idea that

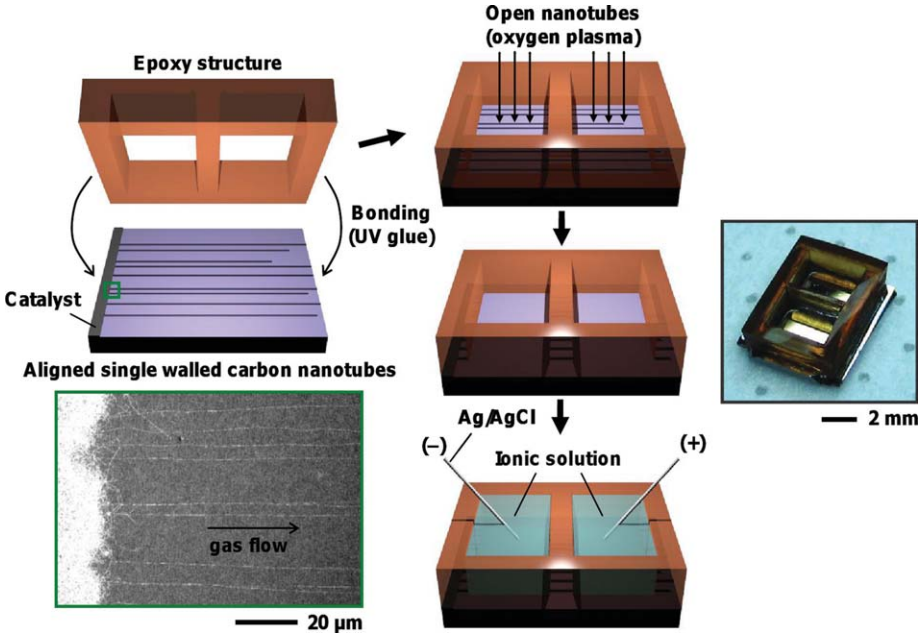

Figure 5. Fabrication of SWCNT ion channels.

An epoxy structure with two compartments is bonded onto a substrate with ultra-long and aligned CVD-grown SWCNTs (SEM image). Etching the unprotected region in oxygen plasma leaves an array of open-ended SWCNTs. Both compartments are filled with ionic solution, and the electro-osmotic current through the SWCNTs is monitored. The epoxy structure serves as a mask during the plasma treatment and also suppresses molecular transport along the SWCNT exterior. Reprinted with permission.[70]

cations are the pore blockers (as opposed to anions) is evidenced by the fact that smaller cation salts (LiCl, NaCl, and KCl) can block these pores, while larger cation salts, such as tetramethylammonium chloride (TMA^+Cl^-), do not cause pore-blocking events.[70]

The experimental evidence of this stochastic pore blocking phenomenon, generated by Choi et al. is shown in Figure 6a for LiCl, NaCl, and KCl.[70–71] A summary of the pore-blocking currents and mobilities shows that each cation exhibits specific ranges of pore-blocking current (related to the change in conductance between the two current states, ΔG), and dwell times that may allow such current traces to be used for molecular identification in sensors.

Besides the stochastic pore blocking, it was observed that current fluctuations through the interior of the nanopore can undergo coherent oscillations, as shown in Figure 6b. The observed oscillations occur because of coupling between pore blocking and a proton-diffusion limitation at the pore mouth shown in the reaction network in Figure 6c, which was modeled using kinetic Monte Carlo simulations. The result illustrates how simple ionic transport can generate coherent waveforms within an inherently noisy environment.

More recent work has analyzed a device with two open tubes, which leads to the observation of a three-state system.[71] A threshold voltage was detected for this device, whereby below this voltage no pore blocking events were observed, which was ascribed to the electrostatic barrier for cation species partitioning into the carbon nanotube pore. This electrostatic barrier is caused by the transfer of charged particles from a high-dielectric solvent (bulk water) to a low-dielectric environment (interior of the carbon nanotube), electrostatic binding to the negatively-charged carboxylate groups near the pore mouth, and the partial shedding of hydration shells for ions entering small, hydrophobic pores. From this study, it was possible to conclude that a simple Markov network with linear electric field dependence (corrected by the threshold voltage) of the translocation velocity approximately describes this system.[71]

This research opens up exciting opportunities for devices and applications utilizing carbon nanotubes as nanoscale conduits. If nanopores undergoing coherence resonance can be synchronized, horizontally-aligned carbon nanotubes embedded in membranes could be used for novel separations which lock on to the frequency of ion transport through the nanotubes, as depicted in Figure 7a. The use of end-group functionalization could also improve nanotube selectivity or allow the fabrication of sensors that detect ions through observation of pore blocking events. It is realistic to envision the production of a probe that would enable detection and identification of single ions in solution, fingerprinted by their pore-blocking current and dwell times, as drawn in Figure 7b. Altogether, this research field will help answer

Table 3. Evidence for Stochastic Pore-Blocking Phenomenon in SWCNT Nanopores

Proposed Characteristics of Stochastic Pore Blocking in CNTs	Experimental Evidence
Protons are main charge carriers	• Conductivity decreases with addition of salt • Increasing pH decreases the pore blocking current • Using D_2O decreases the pore blocking current
Cations are blockers	• Conductivity decreases with addition of salt • Large cation salts (TMA^+Cl^-) do not result in pore blocking events • Experiments with just water or HCl do not yield pore blocking events

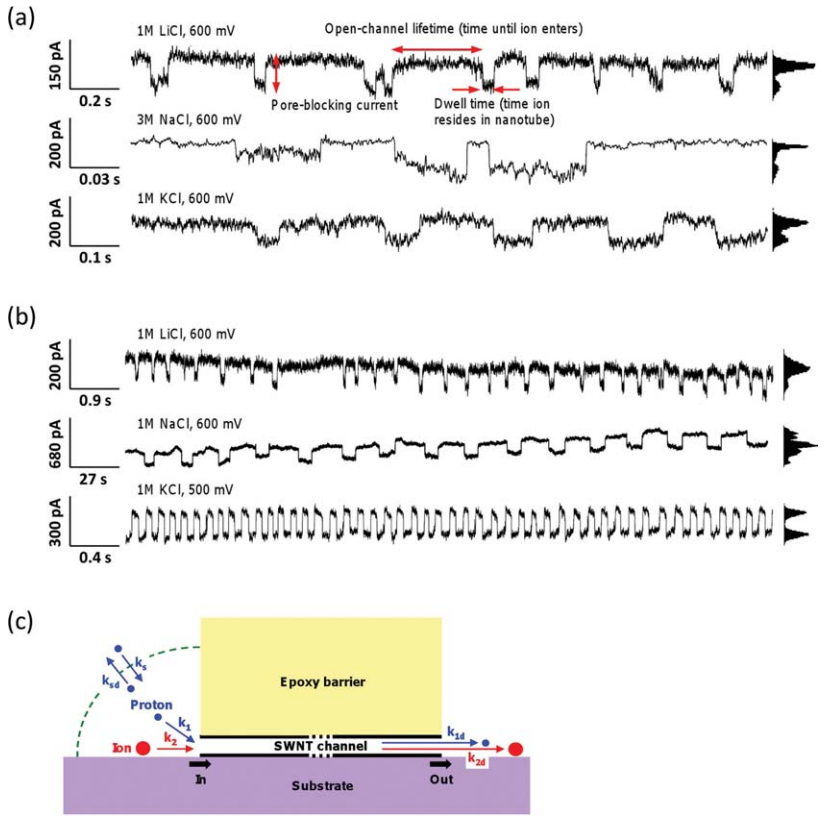

Figure 6. Stochastic pore blocking phenomena.

(a) Example current traces when a constant voltage is applied across the reservoirs of the nanopore device. The top trace depicts the features corresponding to the pore-blocking current, open-channel lifetime, and dwell time. (b) Example current traces of the system under coherence resonance, where ion transport becomes synchronized. (c) A model illustrating the competition between protons and ions entering the nanotube. The diffusion-limitation of protons at the pore mouth can lead to coherence resonance under certain conditions. Adapted with permission.[70]

fundamental questions of transport through carbon nanopores that will enable a new generation of nanofluidic devices and sensors.

The Electron Transfer Chemistry of One- and Two-Dimensional Materials

One- and two-dimensional carbonaceous materials have been shown to participate in a variety of electron transfer chemistries.[74–76] Recently, studies by the authors of this Perspective and by other groups have shown that, for chemistries that are rate-limited by the transfer of electrons from the carbon material to a redox molecule in solution, relative rate constants can be evaluated using Gerischer-Marcus theory.[77–79] This theory states that the rate constant associated with electron transfer is proportional to the degree of overlap between the occupied density of states (DOS) of the electron donor, and the distribution of vacant oxidized states for the solvated redox molecule. An interesting aspect of one- and two-dimensional carbon materials is that their electronic structure can vary significantly depending on the organization of their carbon atoms. Hence, as shown in Figure 8 for two species of carbon nanotubes, the (9,8) species exhibits substantially more overlap with the vacant oxidized states, and will therefore react more readily than the (6,5) species. Such differences in reactivity are also predicted for graphene nanoribbons,[80] and have recently been demonstrated for 2-D graphene sheets, where edge and monolayer carbons display significantly higher reactivity than those of bi- and multilayers.[77] These differences provide for unique opportunities to manipulate carbon materials, both physically and electronically, and have been successfully utilized to separate carbon nanotubes by electronic type.[48,81]

The first structure-reactivity relationship for electron-transfer reactions of single-walled carbon nanotubes was derived and experimentally validated by Nair et al.[78] using 4-hydroxybenzene diazonium as a model electron acceptor. In this work, the slow metering of diazonium solution was utilized in order to operate the reaction in the adsorption-controlled regime, where partial doping of the SWCNT occurs due to the formation of a charge-transfer complex with the diazonium salt.[82–83] Gerischer-Marcus theory, which produced the best fits to the experimental data, states that the rate of reaction is proportional to the degree of overlap between the SWCNT density of states $DOS_{(n,m)}$, and the distribution of oxidized states for the aryl-diazonium molecule in solution W_{ox}

$$k_{ET}^{(n,m)} = \upsilon_n \int_{E_F^D}^{E_F^{SWNT}} \varepsilon_{ox}(E) DOS_{(n,m)}(E) W_{ox}(E) dE \qquad (16)$$

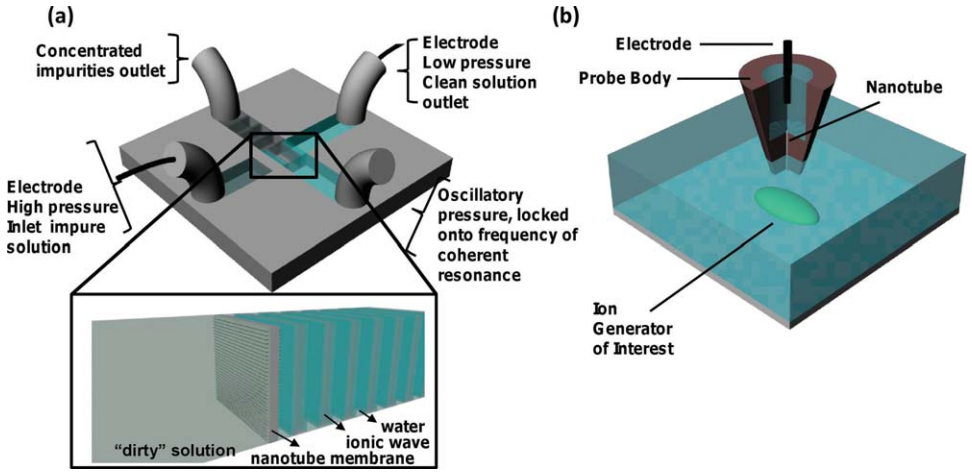

Figure 7. Concept art of future applications.

(a) Incorporating aligned nanotube membranes into microfluidic separators that would allow coherence resonance separations. (b) Incorporation of carbon nanotubes into sensor probes to detect single ions.

Thus, metallic species, which have no band gap, will exhibit the highest reaction rates, followed by small and large band gap semiconductors, respectively. Employing such differences in reactivity one may selectively alter the properties of metallic nanotubes, thereby allowing for separation by electronic type using free-solution electrophoresis[81] and density gradient ultracentrifugation.[48] Recently, this theoretical work was expanded upon by examining these reactions in the limit of sparse functionalization.

While selective at low concentrations, diazonium salts are capable of highly functionalizing all species of nanotubes, disrupting π-conjugation, and destroying the characteristic van Hove singularities. Therefore, it is desirable to be able to controllably introduce a small number of covalent tethers to a carbon nanotube. Considering SWCNT separation alone, such a technique would allow metallic species to be separated from solution while maintaining as much of their intrinsic conductivity as possible. Utilizing the Gerischer-Marcus parameters evaluated from prior work,[78] Hilmer et al. utilized a kinetic Monte Carlo formalism to examine the conditions under which monofunctionalization of carbon nanotubes can be achieved.[84] As might be expected, not only must the degree of conversion be extremely small for this to take place, but the ability to obtain a significant fraction of monofunctional tubes is dependent on the diameter distribution, and, therefore, the distribution of rate constants, in the nanotube solution. Looking at SWCNTs synthesized by three different approaches, Hilmer et al. examined the fundamental limits that can be achieved for separating nanotubes by electronic type.[84] In general, it was found that selective chemistry is increasingly effective as the nanotube solution predominantly contains smaller diameter species. This is due to a greater fraction of larger band gap semiconductors, and, therefore, a larger discrepancy in the reactivities of metallic and semiconducting species.

In addition to these studies on SWCNTs, theoretical investigations on the electron-transfer reactions of graphene nanoribbons have also been carried out.[80] It was found that the reactivities of GNRs depend on both the width of the ribbon and the orientation of carbon atoms along the nanoribbon edge. For cases in which it is possible to use a tight-binding description of the nanoribbon band structure, Gerischer-Marcus theory predicts that the reactivity trends of armchair and zigzag GNRs have opposite dependences on width, with the reactivity of armchair species increasing with width, and that of zigzag GNRs decreasing. For zigzag species, in particular, the major contribution to reactivity stems from the edge states. Therefore, narrow zigzag GNRs are predicted to be the most reactive of all nanoribbon species. As in the case of SWCNTs, such differences in reactivity may be utilized for selective functionalization, or to separate GNRs by type.

In separate work, Raman spectroscopy was used to probe the reactivity of substrate-bound single and multilayer graphene toward derivatization with 4-nitrobenzene diazonium salt.[85] In this study, it was found that graphene monolayers are almost 10 times more reactive than bi- or multilayer graphene, as determined by the relative disorder peak in the Raman spectrum. However, this result contradicts the Gerischer-Marcus theory,

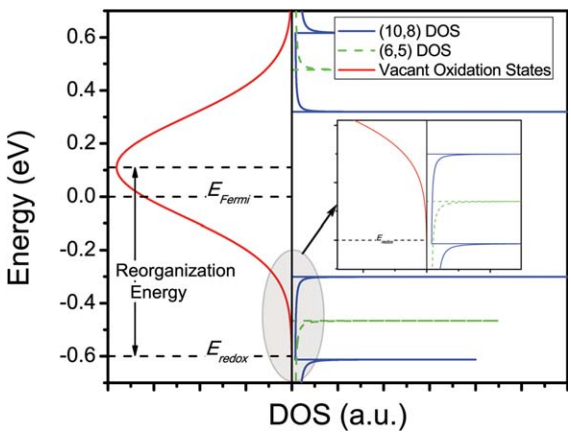

Figure 8. Densities of States (DOS) for two semiconducting nanotube species, evaluated using a third-nearest neighbor tight-binding approximation, along with the vacant oxidized states of a generic redox molecule in solution.

Gerischer-Marcus theory states that the rate constant associated with electron transfer from the nanotube to the redox molecule is proportional to the degree of overlap between the occupied SWCNT DOS and the oxidized states of redox species.

which predicts that a bilayer of graphene should be approximately 1.6 times as reactive as a monolayer. This contradiction can be resolved by considering the potential effects of the substrate, on which local puddles of electrons and holes can shift the Dirac point of the graphene monolayer.[86–88] In addition to examining the differences in reactivity between mono- and multilayer graphene, this study discovered that the reactivity of graphene edges is at least two times greater than that of the bulk. These findings have been confirmed by Raman mapping of graphene surfaces subjected to 4-nitrobenzene diazonium salt.[85]

Such electron transfer chemistries offer great potential for both physically and electronically manipulating the properties of carbon materials. In particular, for carbon nanotube separation, it will be interesting to see how chemistries and protocols can be adapted to meet the proposed limits. In addition, by operating in the regime of low functionalization, either by selectively functionalizing graphene edges, or utilizing stoichiometric control with nanotube solutions, it may be possible to build a hierarchical nanostructure that possesses unique and well-defined properties.

Conclusions

The properties of low-dimensional materials are substantially different from those of their bulk counterparts, and their understanding requires the application of fundamental chemical engineering concepts. These materials are transforming technology in a variety of different fields going all the way from life sciences to energy and to advanced materials. A hexaganol carbon lattice is the basis of the most quintessential LDMs, capable of generating 0-D (fullerenes), 1-D (nanotubes) and 2-D (planar graphene) quantum confined materials, each with a unique set of properties. This review outlines several examples of the chemical engineering of carbon-based LDMs, as summarized below:

1. Self-propagating reaction waves have led to a new energy generation mechanism recently discovered which are called thermopower waves. These waves generate a thermal pulse that drives electrons down an electrically conductive nanostructure, for example, potentially leading to fundamentally new types of batteries and fuel cells.

2. It is essential that excitons be viewed from a chemical engineering perspective and that experimental data from excitonic systems be studied in this light. Reaction engineering concepts can describe their transport and reaction, which has been applied to two recently developed photoelectronic SWCNT-based applications: nanoheterojunction solar cells and exciton antennas that can act as solar concentrators.

3. Monitoring the radiative decay of excitons in SWCNTs also enables a new class of chemical sensors capable of detecting and quantifying the flux of single molecules. The ability to count single molecules emanating from a nanoscale source is unique even among emerging nanosensors, and will lead to new and powerful diagnostics that can be used in the field of life sciences.

4. Molecular transport through the interior of nanotube systems suggests that nanotubes can be effective and selective molecular nanoconduits. Their smooth-lined walls and enormous aspect ratios are unique among nanopores. A number of quite exotic transport behaviors have been uncovered, including coordinated molecular diffusion by way of coherent oscillations. The observation that one can have molecules synchronize their transport across a nanopore may lead to new types of separation mechanisms.

5. Finally, it is essential to realize that the chemical reactivity of SWCNTs, GNRs and graphene, is fundamentally influenced by the unique electronic DOS, resulting from quantum confinement.

Studying LDMs will continue to teach us new chemistry and physics, and most importantly, new ways to apply chemical engineering principles to solve technological problems.

Literature Cited

1. Davies JH. *The Physics of Low-Dimensional Semiconductors*. 6th ed. New York: Cambridge University Press; 2006:1–438.
2. Weisman RB, Bachilo SM. Dependence of optical transition energies on structure for single-walled carbon nanotubes in aqueous suspension: An empirical Kataura plot. *Nano Lett*. 2003;3:1235–1238. doi:10.1021/nl034428i.
3. Yu H. et al. Cadmium selenide quantum wires and the transition from 3D to 2D confinement. *J Am Chem Soc*. 2003;125:16168–16169. doi:10.1021/ja037971.
4. Li LS, Hu JT, Yang WD, Alivisatos AP. Band gap variation of size- and shape-controlled colloidal CdSe quantum rods. *Nano Lett*. 2001;1:349–351, doi:10.1021/nl015559r.
5. Soloviev VN, Eichhofer A, Fenske D, Banin U. Molecular limit of a bulk semiconductor: Size dependence of the "band gap" in CdSe cluster molecules. *J Am Chem Soc*. 2000;122:2673–2674.
6. Cahay ML JP, Lockwood DJ, Bandyopadhay S, Harris JS. Qunatum confinement VI: nanostructured materials and devices. *Electrochem Soc*. 2001;1–398.
7. Zhou X, Dayeh SA, Aplin D, Wang D, Yu ET. Direct observation of ballistic and drift carrier transport regimes in InAs nanowires. *Appl Phys Lett*. 2006:89. doi:10.1063/1.2236589.
8. Li DY, et al. Thermal conductivity of individual silicon nanowires. *App Phys Lett*.2003;83:2934–2936. doi:10. 1063/1.1616981.
9. Lu X, Chu JH. Phonon heat transport in silicon nanowires. *Euro Phys J B*. 2002;26:375–378. doi:10.1140/epjb.e20020102.
10. Lee K, Kim M, Kim H. Catalytic nanoparticles being facet-controlled. *J Mater Chem*. 2010;20:3791–3798. doi:10.1039/b921857b.
11. Wallace PR. The band theory of graphite. *Phys Rev*. 1947;71:622–634.
12. Slonczewski JC, Weiss PR. Band structure of graphite. *Phys Rev*. 1958;109:272–279.
13. Peierls RE. Quelques proprietes typiques des corpses solides. *Ann IH Poincare*. 1935;5:177–122.
14. Landau L. Zur Theorie der phasenumwandlungen II. *Phys Z Sowjetunion*. 1937;11:26–35.
15. Geim AK, Novoselov KS. The rise of graphene. *Nature Mater*. 2007;6:183–191.
16. Partoens B, Peeters FM. From graphene to graphite: Electronic structure around the K point. *Phys Rev B*. 2006;74.doi:10.1103/PhysRevB.74.075404.
17. Berber S, Kwon YK, Tomanek D. Unusually high thermal conductivity of carbon nanotubes. *Phys Rev Lett*. 2000; 4:4613–4616.

18. Purewal MS. et al. Scaling of resistance and electron mean free path of single-walled carbon nanotubes. *Phys Rev Lett*. 2007;98. doi:10.1103/PhysRevLett.98.186808.
19. Martel R, Schmidt T, Shea HR, Hertel T, Avouris P. Single- and multi-wall carbon nanotube field-effect transistors. *Appl Phys Lett*. 1998;73:2447–2449.
20. Saran N, et al. Fabrication and characterization of thin films of single-walled carbon nanotube bundles on flexible plastic substrates. *J Am Chem Soc*. 2004;126:4462–4463, doi:10.1021/ja037273p.
21. Pasquier AD, Unalan HE, Kanwal A, Miller S, Chhowalla M. Conducting and transparent single-wall carbon nanotube electrodes for polymer-fullerene solar cells. *Appl Phys Lett*. 2005;87. doi:10.1063/1.2132065.
22. Wu JB, et al. Organic solar cells with solution-processed graphene transparent electrodes. *Appl Phys Lett*. 2008;92. doi:10.1063/1.2924771.
23. Choi, W. et al. Chemically driven carbon nanotube-guided thermopower waves. *Nat Mater*. 2010;9:423–429.
24. Choi W, Abrahamson JT, Strano JM, Strano MS. Carbon nanotube-guided thermopower waves. *Mater Today*. 2010; 13:22–33.
25. Abrahamson JT, Strano MS. An analytical solution to coupled chemical reaction and thermally diffusing systems: applicability to self-propagating thermopower waves. *J. Phys Chem Lett*. 2010;1:3514–3519.
26. Abrahamson JT, et al. Wavefront velocity oscillations of carbon-nanotube-guided thermopower waves: nanoscale alternating current sources. *ACS Nano*. 2010;5:367–375, doi:10.1021/nn101618y.
27. Nair N, Strano MS. One-dimensional nanostructure-guided chain reactions: Harmonic and anharmonic interactions. *Phys Rev B*. 2009;80:174–301.
28. Pop E, et al. Negative differential conductance and hot phonons in suspended nanotube molecular wires. *Phys Rev Lett*. 2005;95:155505–155508.
29. Liang WY. Excitons. *Phys Edu*. 1970;5:226.
30. Frenkel J. On the transformation of light into heat in solids. *I Phys Rev*. 1931;37:17.
31. Devi LS, et al. Triplet energy transfer in conjugated polymers. I. Experimental investigation of a weakly disordered compound. *Phys Rev B*. 2008;78. doi:10.1103/PhysRevB.78.045210.
32. Lutich A. A. et al. Efficient energy transfer in layered hybrid organic/inorganic nanocomposites: A dual function of semiconductor nanocrystals. *Appl Phys Lett*. 2010;96. doi:10.1063/1.3319838.
33. Skotheim TAR Jr. *Handbook of Conducting Polymers*. 3rd ed. Taylor & Francis Group, LLC: CRC Press; 2007:1–1024.
34. Xu B, Lowe J, Holdcroft S. Non-radiative decay channels in poly(3-hexylthiophene) and poly(3-dodecylthiophene) and how to control them by molecular engineering. *Thin Solid Films*. 1994;243:638–642.
35. Ohkita H, Cook S, Ford TA, Greenham NC, Durrant JR. Monomolecular triplet decay dynamics in fluorene-based conjugated polymer films studied by transient absorption spectroscopy. *J Photochem Photobiol A Chem*. 2006; 182:225–230.
36. Bjorklund TG, Lim SH, Bardeen CJ. Use of picosecond fluorescence dynamics as an indicator of exciton motion in conjugated polymers: Dependence on chemical structure and temperature. *J Phys Chem B*. 2001;105:11970–11977.
37. Mikhnenko OV, et al. Temperature dependence of exciton diffusion in conjugated polymers. *J Phys Chem B*. 2008;112:11601–11604. doi:10.1021/jp8042363.
38. Förster T. Zwischenmolekulare energiewanderung und fluoreszenz. *Annalen Der Physik*. 1948;2:55–75.
39. Miller A, Abrahams E. Impurity conduction at low concentrations. *Phys Rev*. 1960;120:745–755.
40. Ago H, Petritsch K, Shaffer MSP, Windle AH, Friend RH. Composites of carbon nanotubes and conjugated polymers for photovoltaic devices. *Adv Mater*. 1999;11:1281.
41. Kymakis E, Amaratunga GAJ. Single-wall carbon nanotube/conjugated polymer photovoltaic devices. *Appl Phys Lett*. 2002;80:112–114.
42. Ham MH, et al. Evidence for high-efficiency exciton dissociation at polymer/single-walled carbon nanotube interfaces in planar nano-heterojunction photovoltaics. *Acs Nano*. 2010;4:6251–6259. doi:10.1021/nn1019384.
43. Shaw PE, Ruseckas A, Samuel IDW. Exciton diffusion measurements in poly(3-hexylthiophene). *AdvMater*. 2008;20:3516. doi:10.1002/adma.200800982.
44. Kim BJ, Miyamoto Y, Ma BW, Frechet JMJ. Photocrosslinkable polythiophenes for efficient, thermally stable, organic photovoltaics. *Adv Funct Mater*. 2009;19:2273–228. doi:10.1002/adfm.200900043.
45. Paulus GLC, Stano MS. Optical T-matrix and kinetic monte carlo modeling of nanostructured planar heterojunction solar cells. *ACS Nano*. 2011. In Review.
46. Pettersson LAA, Roman LS, Inganas O. Modeling photocurrent action spectra of photovoltaic devices based on organic thin films. *J Appl Phys*. 1999;86:487–496.
47. Scheidler M, et al. Monte Carlo study of picosecond exciton relaxation and dissociation in poly(phenylenevinylene). *Phys Rev B*. 1996;54:5536–5544.
48. Kim WJ, Nair N, Lee CY, Strano MS. Covalent functionalization of single-walled carbon nanotubes alters their densities allowing electronic and other types of separation. *J Phys Chem C*. 2008;112:7326–7331. doi:Doi 10.1021/Jp710919b.
49. Arnold MS, Green AA, Hulvat JF, Stupp S I, Hersam MC. Sorting carbon nanotubes by electronic structure using density differentiation. *Nature Nanotechnol*. 2006; 1:60–65. doi:10.1038/nnano.2006.52.
50. Ghosh S, Bachilo SM, Weisman RB. Advanced sorting of single-walled carbon nanotubes by nonlinear density-gradient ultracentrifugation. *Nature Nanotechnol*. 2010; 5:443–450. doi:10.1038/nnano.2010.68.
51. Han JH, Paulus GLC, et al. Exciton antennas and concentrators from core-shell and corrugated carbon nanotube filaments of homogeneous composition. *Nature Mater*. 2010;9:833–839. doi:10.1038/nmat2832.
52. Qian HH, et al. Exciton transfer and propagation in carbon nanotubes studied by near-field optical microscopy. *Phys Status Solidi B*. 2008;245:2243–2246. doi:10.1002/pssb.200879598.
53. Jin H, Heller DA, Kim JH, Strano MS. Stochastic analysis of stepwise fluorescence quenching reactions on single-walled carbon nanotubes: single molecule sensors. *Nano Lett*. 2008;8:4299–4304.
54. Crochet J, Clemens M, Hertel T. Quantum yield heterogeneities of aqueous single-wall carbon nanotube suspensions. *J Am Chem Soc*. 2007;129;8058–8059. doi:10. 1021/ja071553d.

55. Heller DA, Baik S, Eurell T E, Strano MS. Single-walled carbon nanotube spectroscopy in live cells: Towards long-term labels and optical sensors. *Adv Mater*. 2005;17:2793–2798.
56. Zhang J, et al. Single molecule detection of nitric oxide enabled by d(at)15 dna adsorbed to near infrared fluorescent single-walled carbon nanotubes. *J Am Chem Soc*. 2010;133:567–581. doi:10.1021/ja1084942.
57. Cognet L, et al. Stepwise quenching of exciton fluorescence in carbon nanotubes by single-molecule reactions. *Science*. 2007;316:1465.
58. Siitonen AJ, Tsyboulski DA, Bachilo SM, Weisman RB. Surfactant-dependent exciton mobility in single-walled carbon nanotubes studied by single-molecule reactions. *Nano Lett*. 2010;10:1595–1599. doi:10.1021/nl9039845.
59. Siitonen AJ, Tsyboulski DA, Bachilo SM, Weisman RB. Dependence of exciton mobility on structure in single-walled carbon nanotubes. *J Phys Chem Lett*. 2010;1: 2189–2192. doi:10.1021/jz100749c.
60. Hummer G, Rasaiah JC, Noworyta JP. Water conduction through the hydrophobic channel of a carbon nanotube. *Nature*. 2001;414:188–190.
61. Zhu F, Schulten K. Water and proton conduction through carbon nanotubes as models for biological channels. *Biophys J*. 2003;85:236–244. doi:10.1016/s0006–3495(03)74469–5.
62. Chen Q, et al. Identification of endohedral water in single-walled carbon nanotubes by 1H NMR. *Nano Lett*. 2008;8:1902–1905. doi:10.1021/nl080569e.
63. Gogotsi Y, Libera JA, Guvenc-Yazicioglu A, Megaridis CM. In situ multiphase fluid experiments in hydrothermal carbon nanotubes. *Appl Phys Lett*. 2001;79:1021–1023. doi:10.1063/1.1391228.
64. Holt JK, et al. Fast mass transport through sub-2-nanometer carbon nanotubes. *Science*. 2006;312:1034–1037.
65. Fornasiero F, et al. pH-Tunable ion selectivity in carbon nanotube pores. *Langmuir* 2010;26:14848–14853. doi:10.1021/la101943h.
66. Hinds BJ, et al. Aligned multiwalled carbon nanotube membranes. *Science*. 2004;303:62–65.
67. Dekker C. Solid-state nanopores. *Nat Nano*. 2007;2:209–215.
68. Storm AJ, Chen JH, Ling XS, Zandbergen HW, Dekker C. Fabrication of solid-state nanopores with single-nanometre precision. *Nature Mater*. 2003;2:537–540. doi: http://www.nature.com/nmat/journal/v2/n8/suppinfo/nmat941_S1. html.
69. Li J, et al. Ion-beam sculpting at nanometre length scales. *Nature*. 2001:412;166–169.
70. Lee CY, Choi W, Han J-H, Strano MS. Coherence resonance in a single-walled carbon nanotube ion channel. *Science*. 2010;329:1320–1324.
71. Choi W, Lee CY, Ham M-H, Shimizu S, Strano MS. Dynamics of simultaneous, single ion transport through two single-walled carbon nanotubes: observation of a three-state system. *J Am Chem Soc*. 2010;133:203–205. doi:10.1021/ja108011g.
72. Mann DJ, Halls MD. Water alignment and proton conduction inside carbon nanotubes. *Phys Rev Lett*. 2003; 90:195503.
73. Brewer ML, Schmitt UW, Voth GA. The formation and dynamics of proton wires in channel environments. *Biophys J*. 2001;80:1691–1702. doi:10.1016/s0006–3495(01)76140–1.
74. Banerjee S, Wong SS. Selective metallic tube reactivity in the solution-phase osmylation of single-walled carbon nanotubes. *J Am Chem Soc*. 2004;126:2073–2081. doi:10.1021/ja038111w.
75. Strano MS, et al. Electronic structure control of single-walled carbon nanotube functionalization. *Science*. 2003; 301:1519–1522.
76. Graupner R, et al. Nucleophilic–alkylation–reoxidation: a functionalization sequence for single-wall carbon nanotubes. *J Am Chem Soc*. 2006;128:6683–6689. doi:10. 1021/ja0607281.
77. Sharma R, Baik JH, Perera CJ, Strano MS. Anomalously large reactivity of single graphene layers and edges toward electron transfer chemistries. *Nano Lett*. 2010;10: 398–405. doi:10.1021/Nl902741x.
78. Nair N, Kim WJ, Usrey ML, Strano MS. A structure-reactivity relationship for single walled carbon nanotubes reacting with 4-hydroxybenzene diazonium salt. *J Am Chem Soc* 2007;129:3946–3954. doi:10.1021/Ja068018i.
79. Bard A J, Faulkner LR. *Electrochemical Methods : Fundamentals and Applications*. 2nd ed. New York, NY: John Wiley & Sons; 2001.
80. Sharma, R, Nair N, Strano MS. Structure-Reactivity Relationships for Graphene Nanoribbons. *J Phys Chem C*. 2009;113:14771–14777. doi:10.1021/Jp904814h.
81. Kim WJ, Usrey ML. Strano MS. Selective functionalization and free solution electrophoresis of single-walled carbon nanotubes: Separate enrichment of metallic and semiconducting SWNT. *Chem Mater*. 2007;19:1571–1576. doi:10.1021/Cm061862n.
82. Usrey ML, Lippmann ES, Strano MS. Evidence for a two-step mechanism in electronically selective single-walled carbon nanotube reactions. *J Am Chem Soc*. 2005;127:16129–16135. doi:Doi 10.1021/Ja0537530.
83. Wang HM, Xu JS. Theoretical evidence for a two-step mechanism in the functionalization single-walled carbon nanotube by aryl diazonium salts: Comparing effect of different substituent group. *Chem Phys Lett*. 2009;477: 176–178. doi: 10.1016/j.cplett.2009.06.076.
84. Hilmer AJ, et al. A kinetic Monte Carlo analysis for the production of singularly tethered carbon nanotubes. *Nanotechnol*. 2010;21:495703.
85. Koehler FM, Jacobsen A, Ensslin K, Stampfer C, Stark WJ. Selective chemical modification of graphene surfaces: distinction between single- and bilayer graphene. *Small*. 2010;9999.
86. Galitski VM, Adam S, Das Sarma S. Statistics of random voltage fluctuations and the low-density residual conductivity of graphene. *Phys Rev B*. 2007;76:245405.
87. Hwang EH, Adam S, Das Sarma S. Carrier transport in two-dimensional graphene layers. *Phys Rev Lett*. 2007; 98:186806.
88. Shklovskii BI. Simple model of Coulomb disorder and screening in graphene. *Phys Rev B*. 2007;76. doi:10.1103/Physrevb.76.233411.